Deep origins of chordate midbrain visual processing centers

Cezar Borba[1], Shea Schwennicke[2], Matthew J. Kourakis[3], William C. Smith[1,3,*]

1. Department of Molecular, Cell and Developmental Biology, University of California, Santa Barbara, CA, USA 93106

2. College of Creative Studies, University of California, Santa Barbara, CA, USA 93106

3. Neuroscience Research Institute, University of California, Santa Barbara, CA, USA 93106

* Corresponding author (w_smith@ucsb.edu)

Abstract

Ciona larvae have two visuomotor behaviors, a looming shadow response and negative phototaxis. These are mediated by distinct, but overlapping, two-interneuron relay circuits connecting photoreceptors and motor neurons. We report that both behaviors operate via fold-change detection (FCD) mechanisms. In other words, they respond to relative changes in input, meaning that two stimuli of the same fold-change but different by three orders of illumination magnitude give identical behavioral outputs. However, the two behaviors have different response profiles to varying fold-changes, with the negative phototaxis showing a power-function, while the shadow response is linear. The photoreceptors project to putative FCD circuits in the posterior brain vesicle (pBV), but with different circuit architectures for the two behaviors, likely accounting for the differing behavioral responses. Finally, we speculate from similarities in anatomy, gene expression, and connectivity that the pBV has common origins with processing centers of the vertebrate midbrain, including the optic tectum.

Introduction

Ascidians, which belong to the chordate subphylum Tunicata, have two distinct morphological states (Satoh, 1994). Following a rapid embryogenesis, ascidians hatch as the larval morph. In most ascidian species, larvae are free-swimming and possess a stereotyped chordate body plan consisting of a muscular tail, notochord and dorsal and hollow central nervous system (CNS). The larval stage of ascidians is brief, lasting only hours or days before they settle. Following settling upon a suitable substrate such as a rock or dock piling, the larvae undergo metamorphosis, during which time the body is extensively remodeled to form the derived sessile adult body plan. Because ascidian embryos and larvae more clearly show conserved chordate features, allowing for easier homology comparisons to vertebrates, these stages have been the primary focus of ascidian research. The larval CNS is of particular interest due to the combined features of simplicity and stereotyped chordate properties. The larval CNS is the product of a conserved chordate neurulation program, and once developed, has an anatomy and gene expression pattern with extensive homology to the generalized vertebrate CNS [reviewed in (Hudson, 2016)]. The best characterized ascidian larval nervous system is that of *Ciona*, and despite having only 177 CNS neurons, is subdivided into domains with proposed homology to the vertebrate forebrain [the *Ciona* brain vesicle (BV)], followed posteriorly by putative homologs of the midbrain/hindbrain junction, hindbrain and spinal cord [the *Ciona* neck, motor ganglion (MG), and rostral nerve cord, respectively]. While the assignment of these homology domains remains a subject of discussion [e.g., (Dufour et al., 2006; Ikuta and Saiga, 2007)], the presence of a midbrain homolog in tunicates, including *Ciona*, in particular is unresolved. Based on the expression patterns of several genes, it has been speculated that tunicates lack a midbrain homolog (Cañestro et al., 2005; Holland, 2009, 2017; Ikuta and Saiga, 2007; Lacalli, 2006; Satoh and Levine, 2005; Striedter and Northcutt, 2020; Takahashi and Holland, 2004), while others have reported evidence of a tunicate midbrain homolog (Imai et al., 2002, 2009).

The tasks of the *Ciona* larva are relatively simple: disperse, and then find a suitable settling place - while avoiding predation. A number of larval behaviors have been described in *Ciona* and other ascidians, including a touch response, negative phototaxis, a looming shadow response and negative gravitaxis (Bostwick et al., 2020; Kajiwara and Yoshida, 1985; Salas et al., 2018; Svane and Young, 1989; Tsuda et al., 2003). *Ciona* larvae are equipped with a number of sensory systems, including the mechanosensitive peripheral nervous system, the gravity-sensitive otolith, and the photosensitive ocellus. It is thought that the coronet cells of the *Ciona* BV constitute an additional sensory system - perhaps for hydrostatic pressure (Eakin and Kuda, 1971; Moret et al., 2005a). The ocellus contains two separate photoreceptive systems that mediate different behaviors (Horie et al., 2008; Kourakis et al., 2019; Salas et al., 2018). The first of these systems initiates at the PR-I cluster of 23 photoreceptors. This cluster contains 21 ciliary glutamatergic photoreceptors, one GABAergic photoreceptor, and one dual GABAergic/glutamatergic photoreceptor (Kourakis et al., 2019). These photoreceptors extend their outer segments into the ocellus pigment cell, which provides directional shading, allowing them to discern the direction of light, and thereby mediate negative phototaxis. The PR-I photoreceptors project directly from the ocellus to the posterior BV (pBV) where they synapse onto two distinct clusters of primary interneurons, the six primarily cholinergic *photoreceptor relay neurons* (prRNs) and the eight primarily GABAergic *photoreceptor ascending motor ganglion relay neurons* (pr-AMG RNs). The second photoreceptive system consists of seven ciliary photoreceptors, the PR-IIs, which are mixed GABAergic and dual GABAergic/glutamatergic (Kourakis et al., 2019). The PR-IIs are clustered anterior and adjacent to the PR-Is and are not associated with the pigment cell. This cluster is thus sensitive to

ambient light changes and mediates the looming shadow response. Like the PR-Is, the PR-IIs project directly from the ocellus to the pBV, but synapse exclusively to the pr-AMG RNs (Kourakis et al., 2019; Ryan et al., 2016). We have speculated the PR-I group has a common origin with the vertebrate lateral eyes, while the PR-II might be related to the vertebrate pineal eye, which in larval amphibians and teleosts mediate a similar looming shadow escape response (Jamieson and Roberts, 2000; Yoshizawa and Jeffery, 2008).

Both *Ciona* photosystems respond to changing illumination. While PR-II visuomotor pathway responds directly to changing ambient light (specifically, decreasing light), it is the decrease in light falling on the PR-Is due to pigment cell shading as the larvae faces away from light while performing casting swims that is the cue for negative phototaxis (Mast, 1921; Salas et al., 2018). The neural processing of visual input implicit in these two behaviors is the subject of this manuscript. We report here that the *Ciona* larval CNS processes visual inputs to detect fold-change differences. This is true in both negative phototaxis and the looming shadow response. In fold-change detection (FCD), the response depends only on the relative change in input, and not on the absolute change (Adler and Alon, 2018; Alon, 2019). FCD allows a sensory system to give a consistent response to the same relative change, independent of the ambient conditions, while suppressing noise (Adler and Alon, 2018; Alon, 2019). Additionally, we present data indicating that the pBV is integral in performing the FCD processing. Finally, we note that the convergence of anatomical, molecular, connectomic and behavioral data point to the *Ciona* pBV as sharing homology to the vertebrate midbrain, suggesting a common origin of visual processing centers, such as the vertebrate optic tectum (OT), and thus this function predates the split of the tunicates and the vertebrates.

Results

Fold-change transformation of visual input.

Many biological systems that respond to temporally changing stimuli transform the input to make the system responsive to relative fold-change, rather than to absolute input levels (Adler and Alon, 2018). A fundamental property of FCD is that increases in the fold-change of a stimulus give an increased output, while the same fold-change, but of different absolute values, gives the same output. To investigate *Ciona* photoresponses, 25-hour post-fertilization larvae were first exposed to a fold-change dimming series using a 505 nm LED lamp while recording at far-red (700 nm), as described previously (Bostwick et al., 2020; Kourakis et al., 2019). The series ranged from 3-fold (600 lux to 200 lux) to 60-fold (600 lux to 10 lux) dimming (Figure 1A and SFigure 1). Several parameters were measured: the percent of larvae responding to dim, the reaction time, and the duration, speed, and tortuosity of dimming-induced swims. Movie 1 shows representative responses to 3-, 10- and 60-fold dims. Of these parameters, induced swim duration showed a positive relation to increased fold-change (Figure 1A), while speed and tortuosity were constant across the series (Figure 1B and SFigure 1A). The percent of larvae responding to dimming increased initially with fold change, but plateaued at around 10-fold, and thus did not appear to be a manifestation of FCD behavior (Figure 1C).

While the dimming response is an output of the PR-II pathway, we reported previously that the PR-I photoreceptors become sensitive to ambient light changes in larvae homozygous for the pigmentation mutant *pristine* (*prs*) because they are no longer shielded by the pigment cell (Salas et al., 2018). Moreover, since there are more Group I photoreceptors than Group II (30 versus 7), it is likely that the Group I output predominates in *prs* larvae. One way this is evident is that the dimming-evoked swims of *prs* mutants are straight, as are phototaxis swims, rather than highly tortuous, as is observed in response to dimming in pigmented animals (Salas

et al., 2018). To validate this further, we find that *prs* larvae are more sensitive to dimming at low-light conditions than wild type (Figure 1D). When the fold-change dimming series was performed on *prs* larvae we again observed a positive relationship of swim time to fold-change, but with a significantly different response curve (Figure 1E and SFigure 1D). . The best fit curve for wild-type swim times versus fold-change was a power slope having an $R^2 = 0.98$. While the log slope of this curve also had an $R^2 = 0.98$, the Bayesian information criterion (BIC, see Methods) for a power relationship had the lower score, indicating a better fit (-13 and 17 for power and log, respectively; $R^2 = 0.87$ for linear). The best fitting model for the *prs* swim times is a linear slope having an $R^2 = 1.00$ ($R^2 = 0.92$ and 0.81 for power and log, respectively). These responses to the fold-change dimming series, showing a power relationship for the PR-II pathway and a linear relationship for the PR-I pathway, indicate different circuit mechanisms at play (Adler et al., 2014).

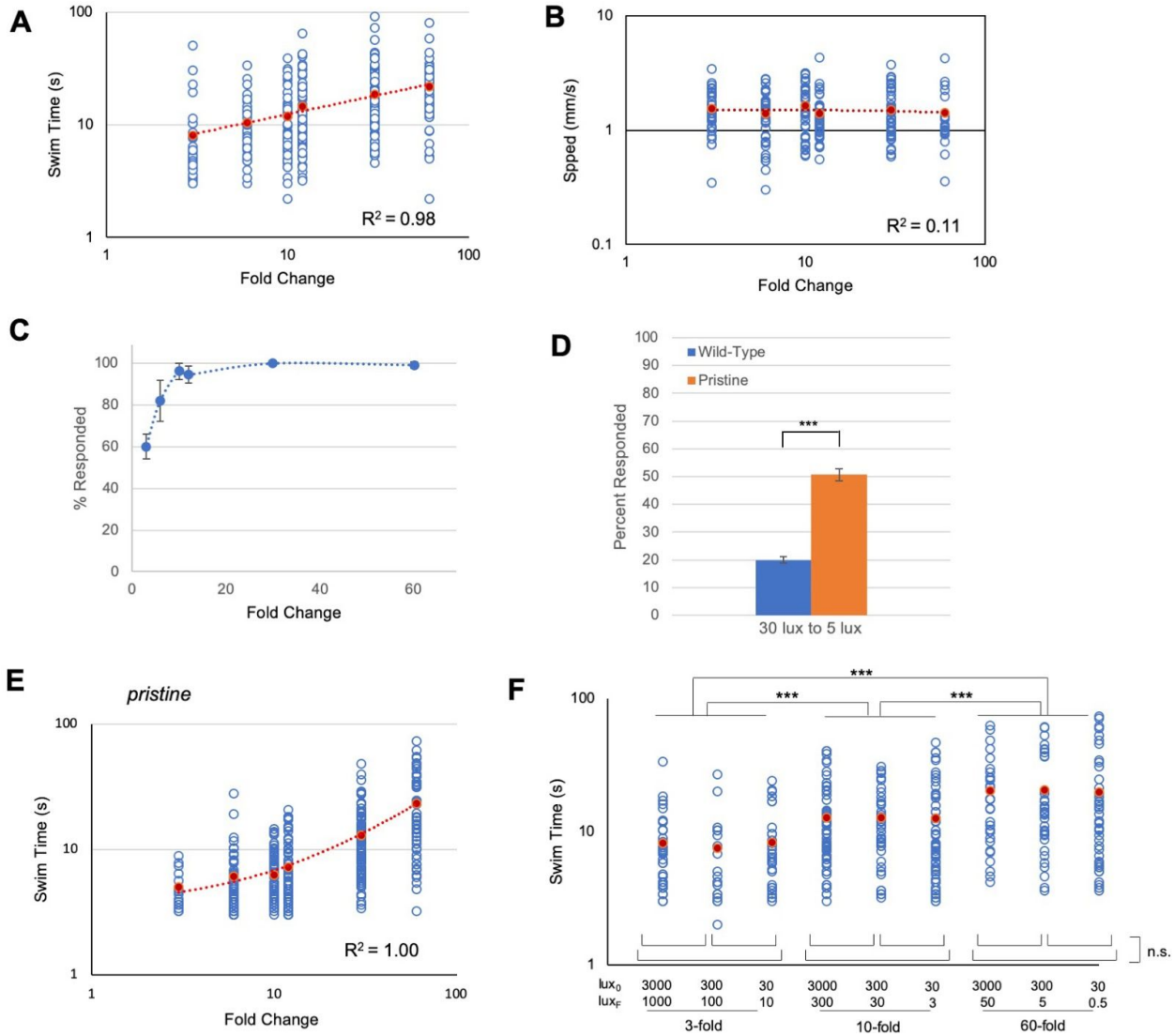

Figure 1. Fold-change detection in *Ciona* photoresponses. **A.** Larval swim times increase as a power function in response to increased fold-change light dimming (3-fold to 60-fold; log/log plot shown). All data points (blue circles) and averages (red circles) are shown (same for panels B, E and F). See also **Movie 1**. **B.** Swim speed is constant across fold-change dimming series.

C. The percent of larvae responding as a function of fold-change dimming. Shown in graph are the averages from three recordings (± S.D.). **D.** Percent of larvae responding to six-fold dim at low illumination conditions (30 lux to 5 lux). *n*= 76 and 131, for wild-type and *pristine*, respectively. **E.** Larval swim times of homozygous *pristine* mutants increase as a linear function in response to increased fold-change light dimming (3-fold to 60-fold; log/log plot shown). **F**. Dimming at same fold-change but different absolute values across three orders of magnitude gives the same swim times. Lux_0: initial illumination level in lux; Lux_F: illumination after dim in lux. (*** = p<0.001; n.s. = not significant). See **SFigure 1** and **2**, including sample sizes, average values, and statistical analyses.

Another of the defining properties of FCD is that stimuli of the same fold-change, but of different absolute magnitudes, will give the same output (Adler and Alon, 2018). We find this holds true for the *Ciona* dimming response across three orders of magnitude. For example, while we observed a significant increase in average swim time between 3-, 10- and 60-fold dims, the swim times between 10-fold dims of 3000 to 300 lux, 300 to 30 lux, and 30 to 3 lux were not different, likewise with 3- and 60-fold dims (Figure 1F and SFigure 2A-B).

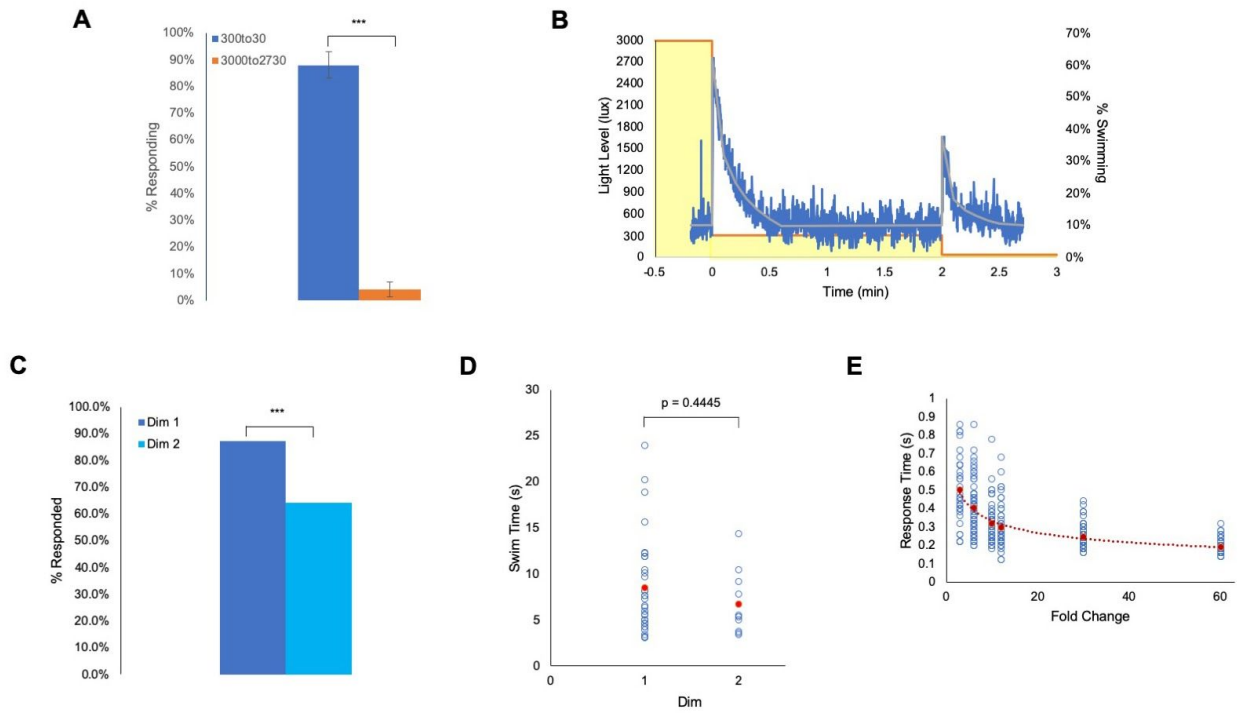

Figure 2. Properties of *Ciona* photoresponse. **A**. The *Ciona* light-dimming response follows Weber's law. Shown are the percent of larvae responding to 270 lux dimming from the initial conditions of 300 lux or 3000 lux (n = 776 and 443; respectively). **B.** *Ciona* larvae show absolute adaptation to light-dimming. Larvae were exposed to two light dimmings separated by two minutes (3000 lux to 300 lux, and 300 lux to 30 lux; yellow boxes). The blue line shows the percent of larvae swimming at 1 second time points (n = 91-320), and the grey line is the average at each time point. See also **Movie 2**. **C.** For data shown in panel B, a higher percentage of larvae responded to the 3000-300 lux dim (Dim 1) than to the 300 to 30 lux dim

(Dim 2). (*** = $p < 0.001$). **D.** For the experiment shown in panel B, the swim times induced by the 3000-300 lux dim (Dim 1) was not different from the 300 to 30 lux dim (Dim 2). **E**. Plot of the reaction time versus fold change. This is defined as the time point at which swimming was first detected following dimming. For panels D and E, all data points (blue circles) and averages (red circles) are shown. See SFigure 2C and D for full data and statistical analyses.

Implied in the response of the larvae to the fold-change series is that they obey Weber's law (*i.e.*, that the change in stimulus needed to elicit a response is proportional to the original stimulus). To demonstrate this directly, larvae adapted to either 3000 lux or 300 lux were then dimmed by 270 lux (*i.e.*, to 2730 or 30 lux, respectively). In those larvae adapted to 3000 lux, we observed no response to the dimming, while in the larvae adapted to 300 lux, we observed vigorous swimming in nearly all larvae (Figure 2A). Another property inherent in FCD systems is exact adaptation [*i.e.*, the system returns to the baseline state even when the modulated stimulus persists at the new state (Shoval et al., 2010)]. To investigate this, larvae were initially adapted to 3000 lux, which was then dimmed to 300 lux and held at this level for 2 minutes. The illumination was then dimmed a second time, to 30 lux (Movie 2). Figure 2B shows a plot of swimming activity of the larvae as illumination levels change. We observed that the larvae respond robustly to the first 10-fold dim (3000 to 300 lux, yellow boxes in Figure 2B), but stop swimming after approximately 30 seconds. The majority of the larvae were then stationary until the second 10-fold dimming (300 to 30 lux). While a lower percent of larvae responded to the second dim than the first (87% vs 64%, Figure 2C), the swim times of responding larvae were the same for both stimuli (Figure 2D). Finally, another predicted property of FCD systems is that the reaction time should be inversely proportional to the fold change (Adler and Alon, 2018), which we observed as a power-slope increase in reaction time as the fold-change decreased (Figure 2E and SFigure 3).

Putative fold-change detection circuits in the posterior brain vesicle

As described in the Introduction, the PR-I and PR-II photoreceptor clusters target a partially overlapping set of primary interneurons in the pBV (Figure 3). The six prRNs receive input exclusively from the PR-Is. *In situ* hybridization and pharmacological studies indicate the prRNs are primarily cholinergic (Kourakis et al., 2019). In contrast, the eight pr-AMG RNs, are mostly (or perhaps exclusively) GABAergic (Kourakis et al., 2019), and are postsynaptic to both the PR-I and GABAergic PR-II photoreceptors (Ryan et al., 2016). There are also extensive synaptic connections between the pr-AMG RNs and the prRNs within the pBV. The PR-I and PR-II circuits then converge on a common set of cholinergic interneurons and motor neurons in the MG (the MGINs and MNs, respectively; Figure 3A). The PR-Is are almost exclusively glutamatergic, and pharmacologic studies confirm that they relay to the MG via the cholinergic prRNs (Kourakis et al., 2019). By contrast, the PR-II circuit is more complex, and a combination of neurotransmitter use, pharmacological and mutant analyses strongly indicates that this pathway activates the MG via disinhibition (Bostwick et al., 2020; Kourakis et al., 2019). When we simplify the PR-I and PR-II circuits by combining cell types and synaptic connections we see the emergence of two likely FCD circuits (Figure 3B). The PR-I circuit (top, Figure 3B) resembles an incoherent feedforward loop predicted to give FCD behavior (Adler et al., 2017) (circuit 04040). The PR-II circuit, being disinhibitory, is more unusual, but strongly resembles a nonlinear integral feedback loop (NLIFL), but with the modulator (m) being excitatory rather than inhibitory (bottom, Figure 3B). Note in the two FCD circuits in Figure 3B that the RN types exchange roles as output and modulator, suggesting an economy of neuron use.

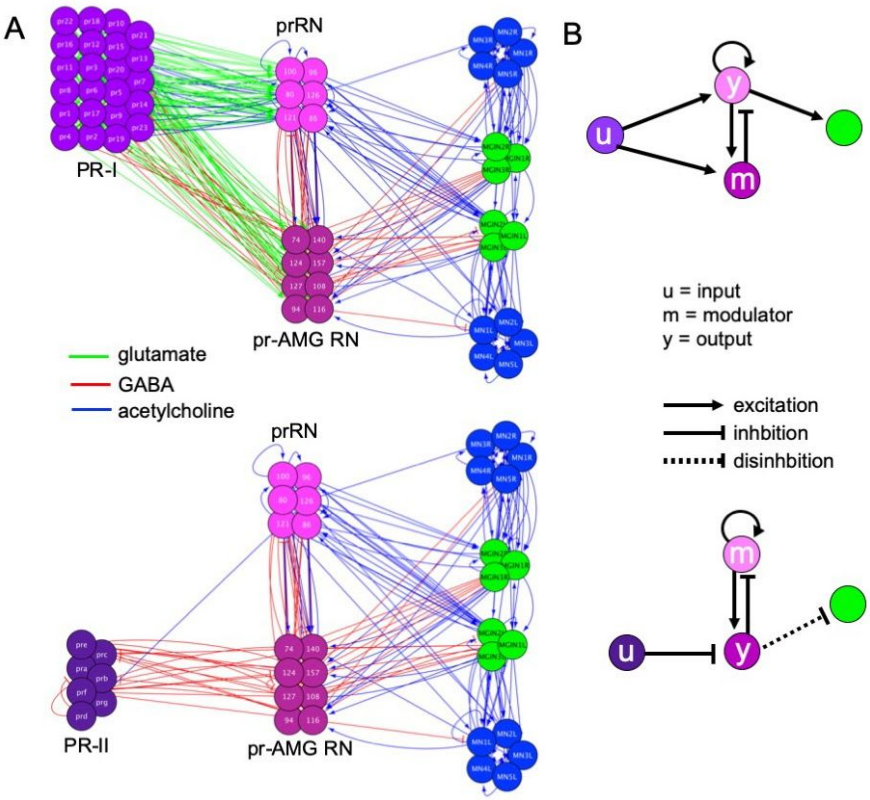

Figure 3. Photoresponse pathways and putative fold-change detection circuits. **A.** Full circuits for the PR-I (top) and PR-II (bottom) pathways from the *Ciona* connectome (Ryan et al., 2016). Neurotransmitter use for synaptic connections (lines) is based on Kourakis et al., 2019. Abbreviations: PR, photoreceptor; prRN, photoreceptor relay neuron, pr-AMG RN, photoreceptor ascending motor ganglion relay neurons; MGIN motor ganglion interneurons; MN motor neurons. **B**. Simplified circuits for the PR-I (top) and PR-II (bottom) pathways derived by combining like cells and assigning valence of synapses (excitatory or inhibitory) based on consensus for that cell type. Nodes are labeled according to proposed function (*i.e.*, input modulator, and output). Colors of nodes and neurons are according to cell-types in Ryan et al., 2016.

To experimentally support the proposed FCD neural circuits, the modulator component of the proposed PR-II FCD dimming circuit was manipulated pharmacologically. In the proposed circuit, the modulators are the cholinergic prRNs (Figure 3B). Previous work showed coexpression of glutamatergic AMPA receptors with VACHT in pBV neurons, but not in GABAergic pBV neurons (Kourakis 2019). We report here that photoreceptors also lack AMPA receptors (Figure 4). The AMPA receptors on the prRNs are targets of the glutamatergic PR-Is, as the AMPA receptor antagonist perampanel inhibits phototaxis, but not the dimming response (Kourakis et al., 2019). Therefore, to selectively modulate the cholinergic prRNs while not directly disrupting the PR-II output, larvae were treated with AMPA (500μM), an agonist of the AMPA receptors. This treatment should result in tonic depolarization of the modulatory prRNs. When assessed in the fold-change dimming series, the percentage of AMPA-treated larvae responding was no different than controls (Figure 5A; SFigure 4A and B). However, the slope of the behavioral response curve in the fold-change series was significantly shallower in the

AMPA-treated sample in comparison to controls (Figure 5B and SFigure 4C-E). In other words, while the larvae still responded to dimming, the change in response between fold-changes was muted, implying the FCD circuit had been manipulated. Figure 5C shows a model of the manipulation. In constant light (left panel), the inhibitory pr-AMG RNs are constitutively active, a prediction of the disinhibition model (Kourakis et al., 2019). In control larvae, dimming results in inhibition of the pr-AMG RNs by the GABAergic PR-IIs, which in turn reduces inhibition of the cholinergic prRNs, setting up the modulator of the FCD circuit (middle panel). With the AMPA present during the dim, the prRNs are tonically depolarized, disrupting their modulatory role in the FCD circuit and resulting in little change between steps in the fold-changes series (right panel). These results are consistent with the proposed FCD circuit architecture for the PR-II pathway. At present we know of no similar pharmacological test of the PR-I FCD circuit.

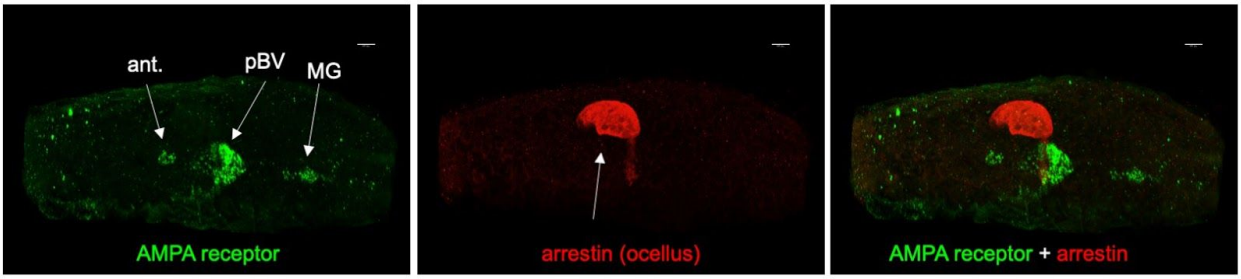

Figure 4. AMPA receptor expression. AMPA receptor expression detected by *in situ* hybridization (green), and the ocellus photoreceptor marker Arrestin was detected by immunostaining (red). Abbreviations: ant., antenna cells; pBV, posterior brain vesicle; MG, motor ganglion.

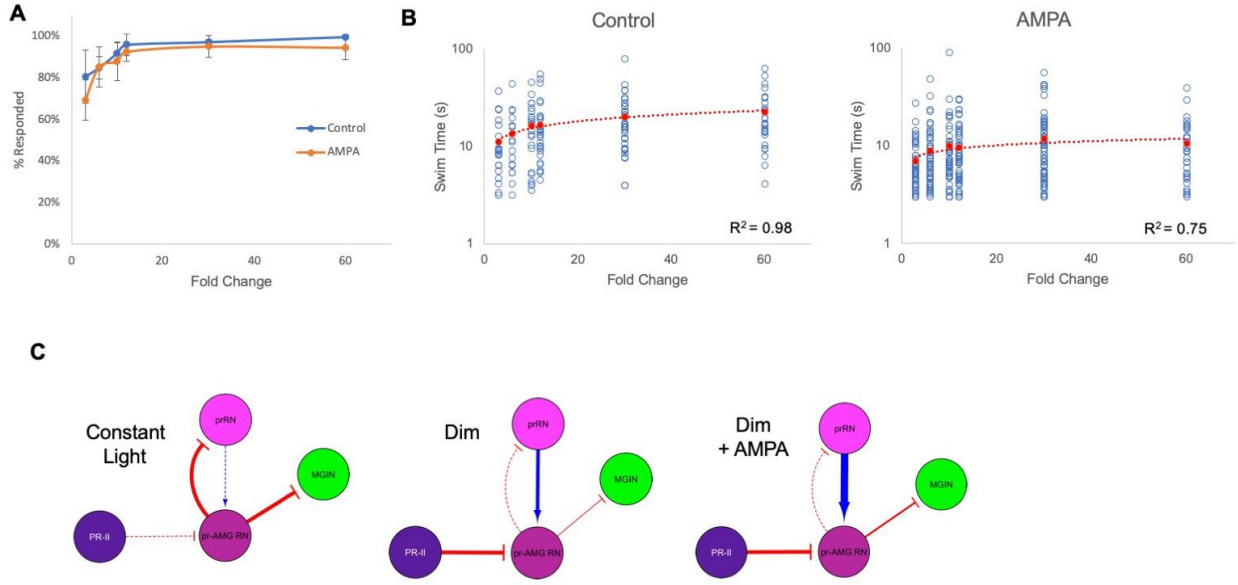

Figure 5. Disruption of PR-II FCD circuit by an AMPA receptor agonist. A. Percentage of control and AMPA-treated larvae responding to the indicated fold-change dimmings. The averages from three recordings are shown (± S.D.). **B.** Swim times of control and

AMPA-treated larvae in the fold-change dimming series. All data points (blue circles) and averages (red circles) are shown. The R^2 valves for the curves are indicated. **C**. Model of AMPA disruption of the PR-II FCD circuit. AMPA treatment gives a tonic depolarization of the modulatory prRNs resulting in greater excition of the output inhibitory pr-AMG RNs. See **SFigure 5** for full data presentation, including sample sizes, average values, and statistical analyses. See also **Movie 3**.

Posterior brain vesicle: homology to the midbrain?

The *Ciona* BV is divided into distinct anterior and posterior domains that derive from invariant cell lineages arising at the 8-cell stage, with the anterior BV (aBV) descending from the a-lineage, and the pBV from the A-lineage (Figure 6A, red and blue cell centroids, respectively) (Nicol and Meinertzhagen, 1988a, 1988b; Nishida and Satoh, 1983). Moreover, the distribution of neuron types is sharply demarcated by this boundary, with the relay neurons, which uniquely project from the BV to the MG, being found only in the pBV. The relay neurons are themselves segregated within the pBV, with those receiving photoreceptor input clustered anteriorly (Figure 6B). We also reported that cholinergic neurons are segregated anteriorly in the pBV, while GABAergic neurons are clustered posteriorly (Kourakis et al., 2019). While it has been proposed that the entire BV has homology to the vertebrate forebrain [see review (Hudson, 2016)], the pBV has a number of features to suggest a link to the vertebrate midbrain, including its anatomical location immediately anterior to the neck region, which is thought to have homology to the vertebrate MHB, and its role in receiving direct input from the visual system. However, the expression patterns of several genes have led to the hypothesis that tunicates either lack, or have lost, a region that shares an origin with the vertebrate midbrain. For example, the gene DMBX, which plays an essential role in vertebrate midbrain development, is not expressed anterior to the MG in *Ciona* (Ikuta and Saiga, 2007; Takahashi and Holland, 2004). In addition, the tunicate *Oikopleura dioica* (Class Larvacea) does not express the genes *engrailed* or *pax2/5/8* anterior to its hindbrain, suggesting that larvaceans lack a midbrain (Cañestro et al., 2005).

Despite the apparent lack of conservation of these few genes, a reevaluation of existing literature, and new data presented here, clearly show that the *Ciona* BV is divided into domains with forebrain and midbrain homology (Figure 6A). Most significantly, *Otx*, which is expressed in the forebrain and midbrain of vertebrates (Boyl et al., 2001), is expressed in *Ciona* in both the aBV and pBV (Hudson et al., 2003; Ikuta and Saiga, 2007; Imai et al., 2002), while a number of the vertebrate forebrain makers are expressed only in the aBV lineage. This includes the genes *Dmrt1* (Kikkawa et al., 2013; Tresser et al., 2010; Wagner and Levine, 2012), as well as the genes *Lhx5*, *Six3*, and *Gsx2* (Reeves et al., 2017; Mazet et al., 2005; Moret et al., 2005b; Esposito et al., 2017), all of which play essential roles in vertebrate forebrain development (Peng, 2006; Lagutin, 2003; Toresson et al.; Kirkeby et al., 2012). While *Gsx2* is also expressed in the pBV, this is only in later stages of development (tailbud stages). Additional vertebrate forebrain markers expressed exclusively in the aBV lineage include *Lhx2/9*, *Bsx* (or *Bsh*) and *Arx* (or *Aristaless*) (Cao et al., 2019). In vertebrates these genes are reported to play essential roles in cortex development (Shetty et al., 2013; Roy et al., 2014; Schredelseker et al., 2020; Marsh et al., 2016).

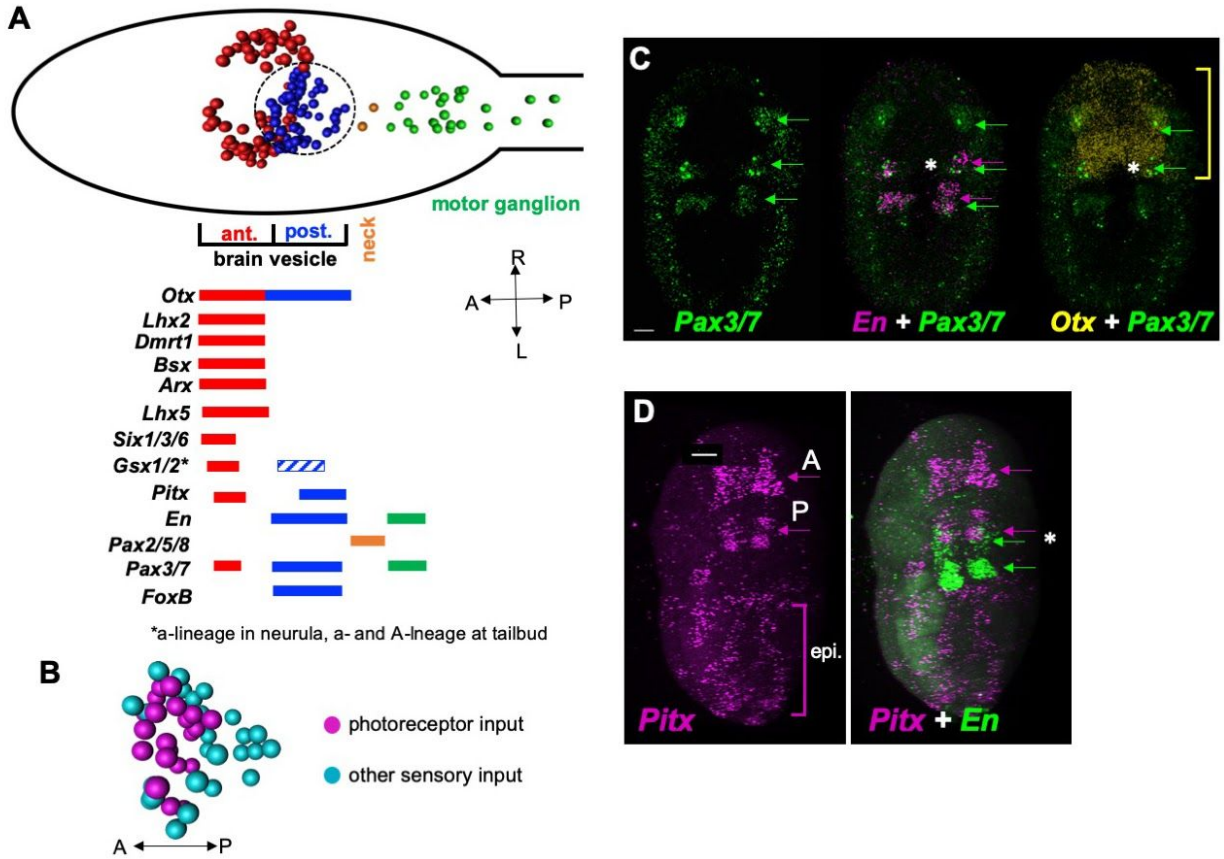

Figure 6. Gene expression in the *Ciona* posterior brain vesicle indicates homology with vertebrate midbrain. A. Top: Diagram of the *Ciona* larval CNS with the major brain regions indicated in color. The centroids of neurons are shown (from Ryan et al., 2016). Bottom: summary of embryonic gene expression patterns marked by corresponding larval CNS domains. **B.** Spatial distribution of relay neuron types in the pBV. Region shown corresponds to the circled area in panel A (centroids shown). **C.** *In situ* hybridization for *Pax3/7*, *En*, and *Otx* in early tailbud *Ciona* embryos. The anterior domain of *En*, which marks the presumptive pBV, overlaps with *Pax3/7* (asterisk middle panel), and *En* (asterisk right panel). **D.** *In situ* hybridization for *Pitx* and *En*. *Pitx* is expressed in anterior and posterior domains in early tailbud embryos. The posterior domain of *Pitx* overlaps with the anterior *En* domain in the pBV (asterisk right panel). Consistent with previous reports, labeling was also observed in the epidermis. Abbreviations: A, anterior; P, posterior; epi, epidermis. Anterior is to the left for panel A and D, and to the top for B and C. Scale bars are 10 microns.

By contrast, the pBV expresses a number of genes associated with the vertebrate midbrain. This includes the A-lineage specific marker *FoxB1* (or *Ci-FoxB*) (Moret et al., 2005b; Oonuma et al., 2016), which in vertebrates plays a role in midbrain development (Wehr et al., 1997). The development of the vertebrate optic tectum, a midbrain structure, requires the co-expression of *pax3*, *pax7*, *Otx2*, and *En* (Matsunaga et al.; Thompson et al., 2008). The *Ciona engrailed* homolog is expressed in two domains embryologically, posteriorly in the MG and anteriorly in the pBV (Ikuta and Saiga, 2007; Imai et al., 2002). We observed overlapping expression of *Pax3/7*, *En*, and *Otx2* in the developing pBV of early tailbud embryos (Figure 6C, asterisk). Finally, *Pitx* has a well-defined role in vertebrate midbrain development (Luk et al.,

2013). We observed *Ciona pitx* expression at early tailbud stage in a posterior domain that overlaps with pBV engrailed expression (Figure 6D, asterisk), as well as in an anterior domain that appears to correspond to the aBV expression reported in older embryos and larvae (Christiaen et al., 2002). In addition, diffuse epidermal labeling was observed, as reported previously (Boorman and Shimeld, 2002). Finally, the pBV is bounded posteriorly by expression of pax2/5/8 in the neck cells, indicating homology with the vertebrate MHB (Ikuta and Saiga, 2007) (Figure 6A).

In summary, the combination of its connectivity, its anatomical location between anterior *dmrt1* and posterior *Pax2/5/8* expression domains, and its expression of *Otx*, *Pax3/7*, *Engrailed* and *Pitx* lead us to conclude that the pBV of *Ciona* is homologous to the vertebrate midbrain.

Discussion

Our behavioral studies show that *Ciona* larvae transform visual input to detect fold-changes. The utility of this behavior is clear: in negative phototaxis, larvae discern the direction of light via casting swims, and it is the change in illumination falling on the PR-Is as the larvae turn away from the light that is the cue to swim. FCD ensures that the casting mechanism functions in the wide range of ambient light conditions that the larva is likely to encounter, and that the response is invariant to the scale of the input. The function of FCD to the dimming response is similar. In the absence of FCD, the change in illumination caused by the same looming object that appeared to be a threat in one ambient light condition, might not in another. FCD ensures that the response varies as a function of the relative shading caused by the looming object. A number of cellular signaling systems have been shown to give FCD responses to extracellular cues, including those in bacterial chemotaxis and growth factor signaling in mammalian cells and embryos (Adler and Alon, 2018; Goentoro and Kirschner, 2009; Lyashenko et al., 2020; Shoval et al., 2010), while modeling has identified several classes of biological circuits that can generate FCD responses (Adler et al., 2017; Goentoro et al., 2009; Hironaka and Morishita, 2014). Here we attempted to identify components of the *Ciona* CNS that could be responsible for the FCD transformation. The *Ciona* photoreceptors themselves certainly play a role in processing the visual inputs. Vertebrate photoreceptors, and in particular cones, have properties that might by themselves generate a FCD output, including adaptation and adherence to Weber's Law (Burkhardt, 1994). However, to our knowledge, FCD by vertebrate photoreceptor phototransduction machinery has not been directly assessed, and modeling suggests that adaptation and adherence to Weber's law alone are not sufficient to give FCD (Shoval et al., 2010), suggesting other processing centers beyond the photoreceptors may be components of this behavior. Moreover, much of the adaptive properties of the vertebrate visual system arises not only from the transduction mechanism inherent to the photoreceptors, but also from the neural circuitry in the vertebrate retina (Dunn et al., 2007). By contrast, *Ciona* ocellus lacks the complex interneuron architecture of the vertebrate retina and the photoreceptors project directly to the pBV.

Several lines of evidence, both published and newly presented here, point to the importance of the pBV in processing visual input. For example, recently published work from our group details the convergence and integration of gravitaxis and visual inputs in the pBV (Bostwick et al., 2020). This multisensory pBV circuit suppresses gravitaxis behavior under constant light conductions, but releases this inhibition in response to dimming. Here we report that further analysis of the *Ciona* connectome and neurotransmitter use (Kourakis et al., 2019; Ryan et al., 2016), indicates that the ocellus photoreceptors project to putative FCD neural circuits in the pBV (Figure 3). Moreover, the architecture of the putative pBV circuits for the PR-I and PR-II pathways are fundamentally different, with the PR-I pathway having a feedforward

motif, while the PR-II pathway has a feedback motif. Modeling of FCD circuits indicates that these different motifs should generate different response curves for varying fold-change (Adler et al., 2017), which agrees well with our observations that the PR-II pathway behaves according to a power rule, while the response in the *prs* mutant, which is dominated by the PR-I pathway, shows a linear relationship (Figure 1). Moreover, if the FCD behavior was the sole product of processing in photoreceptors, this would imply that the phototransduction circuit architecture of the PR-Is and PR-IIs is qualitatively different. While this is not inconceivable, a number of *Ciona* visual cycle components that have been examined (*e.g.*, opsins, arrestin, cellular retinaldehyde-binding protein) are expressed in both photoreceptor groups (Horie et al., 2008; Takimoto et al., 2006). *Ciona* appears to lack an ortholog of the vertebrate rod and cone-specific transducin-type G protein α-subunit, but other α-subunits expressed uniformly in the brain, including in the ocellus, are hypothesized to function in phototransduction (Yoshida et al., 2002). In contrast to the putative FCD circuits for the visual pathway, we find that the gravitaxis pathway in the pBV does not form a plausible FCD circuit (not shown), consistent with the force of gravity being invariant.

Finally, we also show that addition of AMPA changes the slope of the dimming response to the fold-change dimming series (Figure 5). The dimming response appears to operate via a disinhibition mechanism, in which the GABAergic PR-II photoreceptors project to the GABAergic pr-AMG RNs in the pBV (Kourakis et al., 2019). In this behavioral circuit, dimming results in the inhibition of the pr-AMG RNs, which in turn release their inhibition of the excitatory MGIN interneurons in the MG. In the putative FCD circuit for dimming, the modulators are the cholinergic PR-RNs of the pBV (Figure 3). Accordingly, the addition of the AMPA-receptor antagonist perampanel inhibits the PR-I mediated phototaxis, but not the PR-II mediated dimming response (Kourakis et al., 2019). We hypothesize here that by adding AMPA, an agonist, the activity of the circuit modulator should be disrupted, but not the ability of the larvae to respond to dimming. The results are consistent with this hypothesis. Moreover, we found that the AMPA-receptor is not expressed in the ocellus, indicating that the modulator being targeted is not present there. AMPA-receptor expression is observed in both the pBV and the MG (Figure 4). However, the MG does not appear to be a good candidate to contain the FCD circuits. It is dominated by excitatory cholinergic interneurons and motor neurons, while inhibitory neurons, which would be an essential modulatory element of any likely FCD circuit, are limited to the GABAergic AMG neurons, which received no descending input, directly or indirectly, from the photoreceptors or the BV, and the glycinergic decussating ACINs, which likely play a role in the central pattern generator, not visual processing (Kourakis et al., 2019; Nishino et al., 2010; Ryan et al., 2016). In addition, the PR-I and PR-II circuits project from the pBV on a common set of MG interneurons, making it unlikely that this brain region would be responsible for the different fold-change response curves for the PR-I and PR-II circuits.

The evolutionary relationship of the various domains of tunicate larval CNS to those of their vertebrate cousins remains only partially resolved [reviewed in (Hudson, 2016)]. As Figure 6 shows, the *Ciona* BV is derived from two distinct 8-cell lineages, with the aBV descending from the a-lineage, and the pBV descending from the A-lineage. These invariant lineages appear to correspond to fundamental functional subdivisions within the chordate brain, with the aBV expressing genes that mark the forebrain in vertebrates, and the pBV expresses genes associated with the vertebrate midbrain. Moreover, the pBV is the exclusive target of projections from the ocellus photoreceptors, the gravitactic sensory antennae cells, the coronet cells (putative sensory cells), and a subset of peripheral nerves (Ryan et al., 2016, 2018). Thus both by gene expression and connectivity, the pBV shares many of the attributes of the vertebrate midbrain. The results presented here, and those recently published (Bostwick et al., 2020),

indicate that the pBV does not simply relay sensory input to the MG, but rather plays a role in sensory processing and integration. Thus, we can add to the list of similarities between the pBV and the midbrain an apparent conservation of function. These shared features suggest a deeper origin for the antecedents of the vertebrate midbrain processing centers, the OT and pretectum, predating the divergence of tunicate and vertebrate lineages. The presence of a midbrain/OT homologous structure in the most basal chordate group, the cephalochordates (including the model Amphioxus), has been the source of speculation and further studies within this group should provide fertile ground toward the ultimate resolution of the appearance and modification of this structure over time (Lacalli, 2018, 2006).

Methods

Animals.
Wild type *Ciona robusta* (a.k.a., *Ciona intestinalis* type A) were collected from the Santa Barbara harbor. The animals carrying the mutation *pristine* (Salas et al., 2018) were cultured at the UC Santa Barbara Marine Lab (Veeman et al., 2011). Larvae were obtained by mixing dissected gametes of 3 adults and then culturing in natural seawater at 18C. Homozygous *prs* larvae were produced by natural spawning of heterozygous or homozygous *prs* adults.

Hybridization chain reaction (HCR) in situ and immunostaining.
Whole mount *in situ* hybridization of embryonic or larval *C. robusta* were performed as previously described (Kourakis et al., 2019). Briefly, fluorescent labeling was achieved following the hybridization chain reaction (v. 3.0) of Molecular Instruments (Los Angeles). Complementary RNA probe sets were designed to coding regions for the following *C. robusta* genes: *Otx*, *en*, *pax3/7*, *AMPA receptor*, and *pitx*. In larvae which underwent both *in situ* labeling and immunostaining, the *in situ* hybridization was performed first, followed by the immunolabeling (see below), after a transition from 5X SSCT to PBST.

Larvae for immunostaining were dechorionated at mid-tailbud stage using sodium thioglycolate, as for *in situ* hybridization, so that left-right asymmetric properties of the CNS would not be disrupted (Yoshida and Saiga, 2008). The immunostaining followed previously described procedures for *Ciona* (Newman-Smith et al., 2015). A primary antibody against *C. robusta* arrestin (Horie et al., 2005), raised in rabbit, was used at a dilution of 1:1000. A secondary antibody, α-rabbit AlexaFluor 594 (Invitrogen), was also used at 1:1000.

Labeled animals (either by *in situ* or immunohistochemistry) were imaged on an Olympus Fluoview 1000 confocal microscope; post-image analysis used Imaris v5.0 or ImarisViewer v9.5.1 as well as Fiji (ImageJ) v. 2.0.0-rc-69/1.52p.

Behavioral Assays.
All larvae were between 25 and 28 hours post fertilization (hpf) (18°C). Larval swimming behaviors were recorded in sea water with 0.1% BSA using agarose-coated petri dishes to reduce sticking. Image series were collected using a Hamamatsu Orca-ER camera fitted on a Navitar 7000 macro zoom lens. Programmable 700 nm and 505 nm LED lamps (Mightex)

mounted above the petri dishes were used for dimming response assays as previously described (Kourakis et al., 2019). The dim response, adaptation, and reaction time movies were recorded at 5, 8.9, and 50 frames per second (fps), respectively. In the standard assay larvae were recorded for 10s at the initial intensity (lux_0) that was then dimmed (lux_F) to specific values while image capture continued for 2 min. Larvae were allowed to recover for 5 min before being assayed again. All light intensity readings were taken with an Extech Instruments light meter.

Drug Treatments.
(*RS*)-AMPA hydrobromide (Tocris) was dissolved in filtered sea water to a stock concentration of 7.5 mM and then diluted to a final concentration of 500 μM. Larvae were incubated with the drug for about 10 min before beginning assays.

Behavioral Quantification.
Larvae with short bouts of swimming (<3s) were not scored (Bostwick et al., 2020; Kourakis et al., 2019). Swim times, speeds, and tortuosities were calculated using the MATLAB script ELIANE (Kourakis et al., 2019) and the larvae scored between the conditions were tested for significance using the Wilcoxon Rank-Sum test. In the test for absolute adaptation (Figure 2), to measure the percent of larvae swimming at 1 second time intervals, the ELIANE script was modified to determine if a centroid (*i.e.*, larva) in frame x was in the same position in frame x + 1. The sum of moving centroids was then divided by the total number of centroids. Percent of larvae that responded to dimming stimuli was quantified manually and tested for significance using the Student T-Test. R-squared values and Bayesian information criterion (BIC) were calculated using the program R. Larvae that had stuck to the petri dish, or that swam to the edges or into other larvae were not scored.

References

Adler, M., and Alon, U. (2018). Fold-change detection in biological systems. Curr. Opin. Syst. Biol. *8*, 81–89.

Adler, M., Mayo, A., and Alon, U. (2014). Logarithmic and power law input-output relations in sensory systems with fold-change detection. PLoS Comput Biol *10*, e1003781.

Adler, M., Szekely, P., Mayo, A., and Alon, U. (2017). Optimal Regulatory Circuit Topologies for Fold-Change Detection. Cell Syst. *4*, 171-181.e8.

Alon, U. (2019). An Introduction to Systems Biology: Design Principles of Biological Circuits (CRC Press).

Boorman, C.J., and Shimeld, S.M. (2002). Pitx homeobox genes in Ciona and amphioxus show left–right asymmetry is a conserved chordate character and define the ascidian adenohypophysis. Evol. Dev. *4*, 354–365.

Bostwick, M., Smith, E.L., Borba, C., Newman-Smith, E., Guleria, I., Kourakis, M.J., and Smith, W.C. (2020). Antagonistic Inhibitory Circuits Integrate Visual and Gravitactic Behaviors. Curr. Biol. *30*, 600–609.

Boyl, P.P., Signore, M., Annino, A., Barbera, J.P.M., Acampora, D., and Simeone, A. (2001). Otx genes in the development and evolution of the vertebrate brain. Int. J. Dev. Neurosci. *19*, 353–363.

Burkhardt, D.A. (1994). Light adaptation and photopigment bleaching in cone photoreceptors in situ in the retina of the turtle. J. Neurosci. *14*, 1091–1105.
Cañestro, C., Bassham, S., and Postlethwait, J. (2005). Development of the central nervous system in the larvacean Oikopleura dioica and the evolution of the chordate brain. Dev. Biol. *285*, 298–315.
Cao, C., Lemaire, L.A., Wang, W., Yoon, P.H., Choi, Y.A., Parsons, L.R., Matese, J.C., Wang, W., Levine, M., and Chen, K. (2019). Comprehensive single-cell transcriptome lineages of a proto-vertebrate. Nature *571*, 349–354.
Christiaen, L., Burighel, P., Smith, W.C., Vernier, P., Bourrat, F., and Joly, J.-S. (2002). Pitx genes in Tunicates provide new molecular insight into the evolutionary origin of pituitary. Gene *287*, 107–113.
Dufour, H.D., Chettouh, Z., Deyts, C., de Rosa, R., Goridis, C., Joly, J.S., and Brunet, J.F. (2006). Precraniate origin of cranial motoneurons. Proc Natl Acad Sci U A *103*, 8727–8732.
Dunn, F.A., Lankheet, M.J., and Rieke, F. (2007). Light adaptation in cone vision involves switching between receptor and post-receptor sites. Nature *449*, 603–606.
Eakin, R.M., and Kuda, A. (1971). Ultrastructure of sensory receptors in Ascidian tadpoles. Z Zellforsch Mikrosk Anat *112*, 287–312.
Esposito, R., Yasuo, H., Sirour, C., Palladino, A., Spagnuolo, A., and Hudson, C. (2017). Patterning of brain precursors in ascidian embryos. Development *144*, 258–264.
Goentoro, L., and Kirschner, M.W. (2009). Evidence that Fold-Change, and Not Absolute Level, of β-Catenin Dictates Wnt Signaling. Mol. Cell *36*, 872–884.
Goentoro, L., Shoval, O., Kirschner, M.W., and Alon, U. (2009). The Incoherent Feedforward Loop Can Provide Fold-Change Detection in Gene Regulation. Mol. Cell *36*, 894–899.
Hironaka, K., and Morishita, Y. (2014). Cellular Sensory Mechanisms for Detecting Specific Fold-Changes in Extracellular Cues. Biophys. J. *106*, 279–288.
Holland, L.Z. (2009). Chordate roots of the vertebrate nervous system: expanding the molecular toolkit. Nat. Rev. Neurosci. *10*, 736–746.
Holland, L.Z. (2017). 1.01 - Invertebrate Origins of Vertebrate Nervous Systems. In Evolution of Nervous Systems (Second Edition), J.H. Kaas, ed. (Oxford: Academic Press), pp. 3–23.
Horie, T., Orii, H., and Nakagawa, M. (2005). Structure of ocellus photoreceptors in the ascidian Ciona intestinalis larva as revealed by an anti-arrestin antibody. J Neurobiol *65*, 241–250.
Horie, T., Sakurai, D., Ohtsuki, H., Terakita, A., Shichida, Y., Usukura, J., Kusakabe, T., and Tsuda, M. (2008). Pigmented and nonpigmented ocelli in the brain vesicle of the ascidian larva. J Comp Neurol *509*, 88–102.
Hudson, C. (2016). The central nervous system of ascidian larvae. Wiley Interdiscip Rev Dev Biol.
Hudson, C., Darras, S., Caillol, D., Yasuo, H., and Lemaire, P. (2003). A conserved role for the MEK signalling pathway in neural tissue specification and posteriorisation in the invertebrate chordate, the ascidian Ciona intestinalis. Development *130*, 147–159.
Ikuta, T., and Saiga, H. (2007). Dynamic change in the expression of developmental genes in the ascidian central nervous system: revisit to the tripartite model and the origin of the midbrain-hindbrain boundary region. Dev. Biol. *312*, 631–643.
Imai, K.S., Satoh, N., and Satou, Y. (2002). Region specific gene expressions in the central nervous system of the ascidian embryo. Mech Dev *119 Suppl 1*, S275-7.
Imai, K.S., Stolfi, A., Levine, M., and Satou, Y. (2009). Gene regulatory networks underlying the compartmentalization of the Ciona central nervous system. Development *136*, 285–293.

Jamieson, D., and Roberts, A. (2000). Responses of young Xenopus laevis tadpoles to light dimming: possible roles for the pineal eye. J Exp Biol *203*, 1857–1867.
Kajiwara, S., and Yoshida, M. (1985). Changes in Behavior and Ocellar Structure during the Larval Life of Solitary Ascidians. Biol. Bull. *169*, 565–577.
Kikkawa, T., Obayashi, T., Takahashi, M., Fukuzaki-Dohi, U., Numayama-Tsuruta, K., and Osumi, N. (2013). Dmrta1 regulates proneural gene expression downstream of Pax6 in the mammalian telencephalon. Genes Cells *18*, 636–649.
Kirkeby, A., Grealish, S., Wolf, D.A., Nelander, J., Wood, J., Lundblad, M., Lindvall, O., and Parmar, M. (2012). Generation of Regionally Specified Neural Progenitors and Functional Neurons from Human Embryonic Stem Cells under Defined Conditions. Cell Rep. *1*, 703–714.
Kourakis, M.J., Borba, C., Zhang, A., Newman-Smith, E., Salas, P., Manjunath, B., and Smith, W.C. (2019). Parallel visual circuitry in a basal chordate. ELife *8*, e44753.
Lacalli, T. (2018). Amphioxus, motion detection, and the evolutionary origin of the vertebrate retinotectal map. EvoDevo *9*, 6.
Lacalli, T.C. (2006). Prospective protochordate homologs of vertebrate midbrain and MHB, with some thoughts on MHB origins. Int. J. Biol. Sci. 104–109.
Lagutin, O.V. (2003). Six3 repression of Wnt signaling in the anterior neuroectoderm is essential for vertebrate forebrain development. Genes Dev. *17*, 368–379.
Luk, K.C., Rymar, V.V., Munckhof, P. van den, Nicolau, S., Steriade, C., Bifsha, P., Drouin, J., and Sadikot, A.F. (2013). The transcription factor Pitx3 is expressed selectively in midbrain dopaminergic neurons susceptible to neurodegenerative stress. J. Neurochem. *125*, 932–943.
Lyashenko, E., Niepel, M., Dixit, P.D., Lim, S.K., Sorger, P.K., and Vitkup, D. (2020). Receptor-based mechanism of relative sensing and cell memory in mammalian signaling networks. ELife *9*, e50342.
Marsh, E.D., Nasrallah, M.P., Walsh, C., Murray, K.A., Nicole Sunnen, C., McCoy, A., and Golden, J.A. (2016). Developmental interneuron subtype deficits after targeted loss of Arx. BMC Neurosci. *17*, 35.
Mast, S.O. (1921). Reactions to light in the larvae of the ascidians, Amaroucium constellatum and Amaroucium pellucidum with special reference to photic orientation. J Exp Zool *34*, 149–187.
Matsunaga, E., Araki, I., and Nakamura, H. Role of Pax3/7 in tectum development. 9.
Mazet, F., Hutt, J.A., Milloz, J., Millard, J., Graham, A., and Shimeld, S.M. (2005). Molecular evidence from Ciona intestinalis for the evolutionary origin of vertebrate sensory placodes. Dev. Biol. *282*, 494–508.
Moret, F., Christiaen, L., Deyts, C., Blin, M., Joly, J.S., and Vernier, P. (2005a). The dopamine-synthesizing cells in the swimming larva of the tunicate Ciona intestinalis are located only in the hypothalamus-related domain of the sensory vesicle. Eur J Neurosci *21*, 3043–3055.
Moret, F., Christiaen, L., Deyts, C., Blin, M., Vernier, P., and Joly, J.-S. (2005b). Regulatory gene expressions in the ascidian ventral sensory vesicle: evolutionary relationships with the vertebrate hypothalamus. Dev. Biol. *277*, 567–579.
Newman-Smith, E., Kourakis, M.J., Reeves, W., Veeman, M., and Smith, W.C. (2015). Reciprocal and dynamic polarization of planar cell polarity core components and myosin. Elife *4*.
Nicol, D., and Meinertzhagen, I.A. (1988a). Development of the central nervous system of the larva of the ascidian, Ciona intestinalis L. I. The early lineages of the neural plate. Dev.

Biol. *130*, 721–736.
Nicol, D., and Meinertzhagen, I.A. (1988b). Development of the central nervous system of the larva of the ascidian, Ciona intestinalis L. II. Neural plate morphogenesis and cell lineages during neurulation. Dev. Biol. *130*, 737–766.
Nishida, H., and Satoh, N. (1983). Cell lineage analysis in ascidian embryos by intracellular injection of a tracer enzyme. I. Up to the eight-cell stage. Dev Biol *99*, 382–394.
Nishino, A., Okamura, Y., Piscopo, S., and Brown, E.R. (2010). A glycine receptor is involved in the organization of swimming movements in an invertebrate chordate. BMC Neurosci *11*, 6.
Oonuma, K., Tanaka, M., Nishitsuji, K., Kato, Y., Shimai, K., and Kusakabe, T.G. (2016). Revised lineage of larval photoreceptor cells in Ciona reveals archetypal collaboration between neural tube and neural crest in sensory organ formation. Dev. Biol. *420*, 178–185.
Peng, G. (2006). Lhx5 promotes forebrain development and activates transcription of secreted Wnt antagonists. Development *133*, 3191–3200.
Reeves, W.M., Wu, Y., Harder, M.J., and Veeman, M.T. (2017). Functional and evolutionary insights from the *Ciona* notochord transcriptome. Development *144*, 3375–3387.
Roy, A., Gonzalez-Gomez, M., Pierani, A., Meyer, G., and Tole, S. (2014). Lhx2 Regulates the Development of the Forebrain Hem System. Cereb. Cortex *24*, 1361–1372.
Ryan, K., Lu, Z., and Meinertzhagen, I.A. (2016). The CNS connectome of a tadpole larva of Ciona intestinalis (L.) highlights sidedness in the brain of a chordate sibling. Elife *5*, e16962.
Ryan, K., Lu, Z., and Meinertzhagen, I.A. (2018). The peripheral nervous system of the ascidian tadpole larva: Types of neurons and their synaptic networks. J Comp Neurol *526*, 583–608.
Salas, P., Vinaithirthan, V., Newman-Smith, E., Kourakis, M.J., and Smith, W.C. (2018). Photoreceptor specialization and the visuomotor repertoire of the primitive chordate Ciona. J Exp Biol *221*.
Satoh, N. (1994). Developmental biology of ascidians (Cambridge England ; New York: Cambridge University Press).
Satoh, N., and Levine, M. (2005). Surfing with the tunicates into the post-genome era. Genes Dev. *19*, 2407–2411.
Schredelseker, T., Veit, F., Dorsky, R.I., and Driever, W. (2020). Bsx Is Essential for Differentiation of Multiple Neuromodulatory Cell Populations in the Secondary Prosencephalon. Front. Neurosci. *14*, 525.
Shetty, A.S., Godbole, G., Maheshwari, U., Padmanabhan, H., Chaudhary, R., Muralidharan, B., Hou, P.-S., Monuki, E.S., Kuo, H.-C., Rema, V., et al. (2013). Lhx2 regulates a cortex-specific mechanism for barrel formation. Proc. Natl. Acad. Sci. *110*, E4913–E4921.
Shoval, O., Goentoro, L., Hart, Y., Mayo, A., Sontag, E., and Alon, U. (2010). Fold-change detection and scalar symmetry of sensory input fields. Proc Natl Acad Sci U A *107*, 15995–16000.
Striedter, G., and Northcutt, R.G. (2020). Brains Through Time: A Natural History of Vertebrates (Oxford University Press).
Svane, I.B., and Young, C.M. (1989). The ecology and behavior of ascidian larvae. Mar Biol Rev *27*.
Takahashi, T., and Holland, P.W.H. (2004). Amphioxus and ascidian Dmbx homeobox genes give clues to the vertebrate origins of midbrain development. Development *131*,

3285–3294.
Takimoto, N., Kusakabe, T., Horie, T., Miyamoto, Y., and Tsuda, M. (2006). Origin of the Vertebrate Visual Cycle: III. Distinct Distribution of RPE65 and β-carotene 15,15′-Monooxygenase Homologues in Ciona intestinalis†. Photochem. Photobiol. *82*, 1468–1474.
Thompson, J.A., Zembrzycki, A., Mansouri, A., and Ziman, M. (2008). Pax7 is requisite for maintenance of a subpopulation of superior collicular neurons and shows a diverging expression pattern to Pax3 during superior collicular development. BMC Dev. Biol. *8*, 62.
Toresson, H., Potter, S.S., and Campbell, K. Genetic control of D-V identity in the telencephalon. 11.
Tresser, J., Chiba, S., Veeman, M., El-Nachef, D., Newman-Smith, E., Horie, T., Tsuda, M., and Smith, W.C. (2010). doublesex/mab3 related-1 (dmrt1) is essential for development of anterior neural plate derivatives in Ciona. Development *137*, 2197–2203.
Tsuda, M., Sakurai, D., and Goda, M. (2003). Direct evidence for the role of pigment cells in the brain of ascidian larvae by laser ablation. J Exp Biol *206*, 1409–1417.
Veeman, M.T., Chiba, S., and Smith, W.C. (2011). Ciona genetics. Methods Mol Biol *770*, 401–422.
Wagner, E., and Levine, M. (2012). FGF signaling establishes the anterior border of the Ciona neural tube. Development *139*, 2351–2359.
Wehr, R., Mansouri, A., de Maeyer, T., and Gruss, P. (1997). Fkh5-deficient mice show dysgenesis in the caudal midbrain and hypothalamic mammillary body. Dev. Camb. Engl. *124*, 4447–4456.
Yoshida, K., and Saiga, H. (2008). Left–right asymmetric expression of Pitx is regulated by the asymmetric Nodal signaling through an intronic enhancer in Ciona intestinalis. Dev. Genes Evol. *218*, 353–360.
Yoshida, R., Kusakabe, T., Kamatani, M., Daitoh, M., and Tsuda, M. (2002). Central Nervous System-specific Expression of G Protein α Subunits in the Ascidian Ciona intestinalis. Zoolog. Sci. *19*, 1079–1088.
Yoshizawa, M., and Jeffery, W.R. (2008). Shadow response in the blind cavefish Astyanax reveals conservation of a functional pineal eye. J Exp Biol *211*, 292–299.

Acknowledgments

The work was supported by an award from the NIH (NS103774) to W.C.S, and a CCS Create Fund Summer Fellowship to S.S.. We thank Takehiro Kusakabe for the anti-Arrestin antibody.

Author contributions.
C.B. and M.J.K. contributed to experimental design, data collection and analysis, and manuscript preparation. S.S. contributed to data collection and analysis. W.C.S. contributed to research funding, experimental design, data collection and analysis, and manuscript preparation.

Competing interests. The authors declare no competing interests.

A

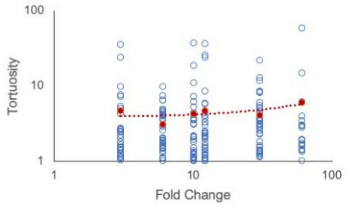

B

Experimental *n*-values

Fold Change	WT Swim Time	*prs* Swim Time	Speed	Tortuosity	% Respond
3	38	15	29	29	127
6	44	56	36	36	102
10	53	70	35	35	105
12	68	72	36	36	125
30	79	90	41	41	132
60	48	56	20	20	143

C

Experiment Averages ± Standard Deviation

Fold Change	WT Swim Time	*prs* Swim Time	Speed	Tortuosity	% Respond
3	8.07±9.15	4.97±1.82	1.56±0.99	4.75±14.69	60.06±5.95
6	10.45±6.30	6.07±4.22	1.40±0.98	3.12±14.27	81.94±9.89
10	11.88±7.95	6.24±2.78	1.65±0.96	4.30±13.85	96.16±4.01
12	14.63±11.38	7.19±4.40	1.41±0.94	4.70±13.48	94.61±4.06
30	18.70±14.80	12.84±8.26	1.51±0.92	4.14±13.15	100.00±0.00
60	21.86±13.98	23.30±15.99	1.42±0.90	6.07±12.82	99.19±1.41

D

Statistical Test *p*-values

WT Swim Times

FC	3	6	10	12	30
6	4.29E-04				
10	2.79E-04	0.2665			
12	1.41E-05	0.0223	0.1093		
30	1.34E-07	1.78E-05	2.67E-04	0.0088	
60	1.77E-07	2.17E-07	2.56E-06	1.18E-04	0.0194

prs Swim Times

FC	3	6	10	12	30
6	0.2721				
10	0.035	0.0565			
12	0.0464	0.0446	0.3559		
30	1.09E-06	7.99E-12	1.74E-11	1.12E-08	
60	5.89E-08	1.46E-14	8.21E-16	1.04E-13	5.85E-06

Speed

FC	3	6	10	12	30
6	0.4095				
10	0.8292	0.2206			
12	0.2222	0.7740	0.2385		
30	0.5197	0.7323	0.5048	0.6867	
60	0.1895	0.7517	0.2446	0.5901	0.4024

Tortuosity

FC	3	6	10	12	30
6	0.7665				
10	0.6563	0.5011			
12	0.7365	0.5849	0.9587		
30	0.2379	0.4717	0.1595	0.1269	
60	0.5085	0.9932	0.6058	0.5668	0.6727

% Respond

FC	3	6	10	12	30
6	0.0304				
10	0.0010	0.0823			
12	0.0011	0.1096	0.6618		
30	0.0003	0.0342	0.1729	0.0832	
60	0.0004	0.0404	0.2854	0.1390	0.3739

Fold-Change	WT vs. PRS
3	0.6642
6	2.05E-06
10	9.94E-07
12	5.14E-08
30	0.0018
60	0.8962

SFigure 1. Expanded data for fold-change assays (Figure 1 panels A-C and E). **A**. Swim tortuosity (Salas et al., 2018) plotted as a function of fold-change dimming. **B.** Number of larvae analyzed in plots of swim time [wild type (WT) and *pristine (prs)*], speed, percent response, and tortuosity versus fold-change dimming. **C**. Experimental averages in plots swim time for WT and *prs*, velocity and tortuosity versus fold-change dimming. **D**. Pairwise tests for significance at each fold-change for swim time (WT and *prs*), speed, percent response and tortuosity (p-values shown; all comparisons by Wilcoxon, except percent response, which was done by T-test). Also shown is a comparison of swim times in WT and *prs* larvae at each fold-change step. P-values for each comparison are listed. FC = fold change.

A

Experiment Data

Fold Change	3-fold			10-fold			60-fold		
Δlux	3000to1000	300to100	30to10	3000to300	300to30	30to3	3000to50	300to5	30to0.5
Average ± SD	8.23±5.89	7.49±6.42	8.35±5.74	12.81±9.41	12.74±7.95	12.56±10.90	20.32±15.43	20.61±16.86	19.92±19.55
n	39	19	34	62	39	54	31	34	43

B

Statistical Test p-values

within fold changes

3-fold	3000to1000	300to100
300to100	0.7327	
30to10	0.3187	0.4726

10-fold	3000to300	300to30
300to30	0.7246	
30to3	0.2942	0.2705

60-fold	3000to50	300to5
300to5	0.2737	
30to0.5	0.8595	0.3729

between fold changes

	3-fold	10-fold
10-fold	1.88E-05	
60-fold	4.36E-11	2.79E-04

SFigure 2. Expanded data for fold-change assay (Figure 1 panel F). A. Average swim times, standard deviations, and number of larvae analyzed for data presented in Figure 1F. **B. Left.** Comparisons of swim times in assays with same fold-change, but different absolute illumination values each fold-change. **Right.** Comparisons of pooled swim times at 3-, 10-, and 60-fold dimming. All tests of significance by Wilcoxon. P-values shown.

A

Experiment Data for response times

Fold-Change	Average ± SD	n
3	0.50±0.17	39
6	0.40±0.14	65
10	0.32±0.10	64
12	0.30±0.11	55
30	0.25±0.06	52
60	0.19±0.04	49

B

Statistical Test p-values for response times

FC	3	6	10	12	30
6	3.80E-03				
10	2.56E-08	1.65E-04			
12	2.45E-08	5.39E-06	0.0701		
30	5.14E-12	2.51E-11	7.00E-06	0.009	
60	1.03E-14	1.91E-17	5.01E-15	2.30E-10	2.28E-07

SFigure 3. Expanded data for reaction time as a function of fold-change. **A.** Average reaction times at the indicated fold changes (± S. D.)**.** The number of larvae analyzed at each fold-change is indicated. **B.** Statistical test of significance for reaction times between fold-changes (p-values shown; Wilcoxon).

A **Percent Responding**: Experiment Averages ± Standard Deviation

Fold Change	Control	AMPA
3	69.15±9.69	80.51±12.88
6	85.08±9.64	84.73±5.41
10	87.81±9.20	91.85±4.73
12	92.49±4.57	95.77±5.06
30	95.04±5.07	97.16±1.24
60	94.51±5.94	99.59±0.70

B **Percent Responding**: p-values for pairwise comparisons

Fold Change	Control vs. AMPA
3	0.2890
6	0.9588
10	0.5360
12	0.4517
30	0.5201
60	0.2153

C **Swim Times**: Experiment Averages ± Standard Deviation

	AMPA		Control	
Fold Change	Swim Time	n	Swim Time	n
3	6.97±4.58	47	11.24±8.24	22
6	8.86±7.77	57	13.55±10.29	17
10	9.96±12.82	51	16.44±11	22
12	9.56±7.15	57	16.6±12.69	31
30	11.79±10.63	72	20.04±13.75	37
60	10.58±7.68	36	22.59±13.77	30

D **Swim Times**: Comparisons within treatments (p-values)

AMPA

FC	3	6	10	12	30
6	0.1340				
10	0.0680	0.3932			
12	0.0332	0.2563	0.3343		
30	0.0023	0.0343	0.0620	0.1397	
60	0.0089	0.0801	0.1145	0.1971	0.5570

Control

FC	3	6	10	12	30
6	0.3100				
10	0.0422	0.1977			
12	0.0216	0.1883	0.5144		
30	5.11E-04	0.0181	0.1775	0.0561	
60	1.36E-04	0.0051	0.0515	0.0122	0.1737

E **Swim Times**: Comparisons between treatments (p-values)

AMPA vs Control	
3-fold	0.0074
6-fold	0.0257
10-fold	4.30E-03
12-fold	5.40E-04
30-fold	2.54E-05
60-fold	1.46E-05

SFigure 4. Expanded data for AMPA-treated larvae. A. Average number of control and AMPA-treated larvae responding to the indicated fold-dimming (± S. D.). Averages are from three recordings. **B.** Statistical comparison of percent of control and AMPA-treated larvae responding at the indicated fold-dimming (p-values; T-test). **C.** Average swim times (± S. D.) and sample sizes for APMA-treated and control larvae. **D.** Comparison of swim times between fold-changes within the AMPA-treated and control groups (p-values are indicated). **E.** Comparison of swim times at each fold-change between the AMPA-treated and control groups (p-values are indicated). FC = fold change.

Movie 1. Response of *Ciona* larvae to 3-, 10- and 60-fold dimming. Video plays at 5X normal speed.

Movie 2. Absolute adaptation. Larvae are exposed to two dimming events separated by 2 minutes. The first dim is from 3000 to 300 lux, and the second from 300 lux to 30. Video plays at 5X normal speed.

Movie 3. Response of APMA-treated and control larvae to a 60-fold dim. Video plays at 5X normal speed.